Observations of quiet solar features with the SSRT and NoRH

Victor V. Grechnev, Arcady M. Uralov, Vladimir P. Maksimov, Vasiliy G. Zandanov,
Gennady Ya. Smolkov, Alexander T. Altyntsev, Boris B. Krissinel,
Nadezhda N. Kardapolova, Sergey V. Lesovoi, Boris I. Lubyshev,
Dmitry V. Prosovetsky, and Georgy V. Rudenko
Institute of Solar-Terrestrial Physics, Lermontov Street 126, Irkutsk 664033, Russia
grechnev@iszf.irk.ru

Abstract

We demonstrate observations of such well-known relatively quiet solar features as filaments & prominences, coronal holes, bright points, and arcades with two radioheliographs, SSRT at 5.7 GHz and NoRH at 17 GHz. Simultaneous microwave observations with the two radioheliographs are promising and fruitful due to overlapping observational daytimes and three times different frequencies. Last circumstance determines significantly different coronal contribution at those frequencies, which governs dissimilar appearance of coronal features in images produced by the NoRH and SSRT. The emphasis is made on SSRT observations, which are not yet well known. We overview some results obtained with the two radioheliographs and discuss new opportunities of radioheliographic observations. Microwave observations are also compared with magnetograms. Only observations at several radio frequencies assure correct estimates of the magnetic field.

Key words: Sun: corona — Sun: radio radiation — Sun: magnetic fields

1. Introduction

The Sun is well known to be extremely variable. There hardly exist a feature on the Sun, which could be quiet absolutely; hence, it would be, probably, more correct to say that we will discuss *relatively* quiet solar features.

The Nobeyama Radioheliograph (NoRH, Nakajima et al. 1994) and the Siberian Solar Radio Telescope (Fig. 1; SSRT, Smolkov et al. 1986; the recent state and data of the SSRT were presented by Grechnev et al. 2003) are among the World's largest radio heliographs dedicated exclusively to solar observations. They have been operating simultaneously for the solar cycle. The SSRT (5.7 GHz) and NoRH (17 & 34 GHz) observe the Sun with a large overlapping of their observational daytimes (local noon at NoRH is at ∼02:45 UT, at the SSRT it is at about ∼05:15 UT), but at very different frequencies. Observations of the quiet Sun at 34 GHz with the NoRH are not straightforward because of the absence of the fundamental spacing at this frequency. Therefore, our discussion is related to NoRH observations at 17 GHz only. The data acquired at these frequencies supply information about coronal processes at different heights in the corona and give an opportunity to estimate contributions of various radio emission mechanisms.

Solar radio emissions in microwaves originate primarily in the solar corona, with some contribution from the transition region, both on the solar disk and above the limb. Thermal free-free emissions are well known to be the major contributor in microwaves. The magnetic field strengths in the corona overlying sunspots are such that gyroresonant absorption at low harmonics of the electron gyrofrequency leads to large optical thicknesses at frequencies below ∼5 GHz. Therefore, emission at the SSRT working frequency is characterized by a relatively large contribution of gyroresonance and thermal free-free emission with respect to the NoRH. A high contrast of radio sources relative to the quiet Sun is typical of the SSRT working frequency. The brightness temperature of steady radio sources in active regions sometimes exceeds 2 MK at 5.7 GHz.

Due to the directly-imaging operating principle of the SSRT, its beam pattern has a relatively low level of sidelobes ($\leq 22\%$ with an ideal field distribution). This allows using even "dirty" SSRT images when there are no very bright sources. However, under their presence, the input dynamic range of the SSRT receiver system becomes very high, unlike the NoRH; in this situation, "cleaning" SSRT images is also necessary. From spring 2000 on, the CLEAN routine has been introduced for SSRT images (Fig. 2). However, the cleaning SSRT images is still not perfect, because 1) the phase distribution over the aperture is not well known, and 2) some geometrical distortions are present, which make difficult cleaning the whole frame with a single beam pattern. For all those reasons, just the relatively quiet solar features of rather low contrast are the most favorable objects to observe with the SSRT.

The SSRT and NoRH observe the quiet Sun, filaments and prominences, coronal holes and bright points, features in active regions such as plages, sunspot-associated sources and neutral line-associated sources. High-sensitivity intensity and polarization observations of gyroresonance and free-free emissions with two-dimensional spatial resolution provide a powerful means by which the structure and dynamics of coronal magnetic fields can be

Fig. 1. View of the SSRT antenna array.

studied (Felli, Lang, Willson 1981; Kundu 1985; Gelfreikh, Pilyeva, Ryabov 1997).

2. Advantages of Observations with Two Radioheliographs

2.1. Two-frequency observations

Radio telescopes supply images of relatively poor spatial resolution with respect to spaceborne thermal imagers, especially those observing in single spectral lines (e.g., SOHO/EIT, TRACE). Besides instrumental limitations, there is a physical reason for that. For the major emission mechanism, thermal free-free emission, the optical thickness is determined by a well-know expression $\tau \propto n_e^2 L T^{-3/2} \nu^{-2}$, with ν being the observing frequency, n_e the electron density, L the depth of the emitting source, and T its temperature. In the optically thin case, this results in very weak temperature dependence $T_B \propto T^{-1/2}$ and, correspondingly, to smearing out the spatial structures observed due to multi-temperature plasmas localized along the line of sight.

However, in the optically thick case, the observed brightness temperature is almost equal to the kinetic temperature, which provides temperature measurements, if we are certain about $\tau \gg 1$. So, on the other hand, these circumstances determine good opportunities for plasma diagnostics, which is the first advantage of observations with two radioheliographs at distant frequencies, because the optical thickness for free-free emission recorded with the NoRH and SSRT differs by about one order of magnitude. Furthermore, the quiet coronal contribution is on the average about 6 000 K on the disk at 5.7 GHz, and it is one order of magnitude lower at 17 GHz, which determines different contrast of the features observed at the two frequencies.

2.2. Other opportunities

- When two-frequency observations are available, we can obtain hints on the presence of non-thermal emissions.
- Significant overlapping in observational daytimes of the SSRT and NoRH provides us with simultaneous observations, which allows realizing the above advantages.
- Finally, observations with two radioheliographs, whose operation principles are very different (synthesis for the NoRH and direct imaging for the SSRT), simplify detection of instrumental contributions, when the features of interest appear dissimilar in their images.

3. SSRT & NoRH Images Compared with Other Observations

Figure 3 shows an example of SSRT (a) and NoRH (c) observations in total intensity close to the previous solar minimum, on October 6, 1997 (from Grechnev et al. 2003), along with Hα images (Big Bear Solar Observatory, b) SOHO/EIT images at 304 Å (d) and 171 Å (e), and the *Yohkoh*/SXT image (f). The images produced with the SSRT, NoRH, and *Yohkoh*/SXT are averaged to enhance the sensitivity, and all the images are nonlinearly

Table 1. Some parameters of the NoRH and SSRT.

	NoRH	SSRT
Configuration	Non-equidistant T	Equidistant Cross
Number of antennas	84	256
Operating frequencies	17 & 34 GHz	5.7 GHz
Main modes	2D snapshots	2D imaging & 1D fast scanning
Angular resolution	10″ @ 17 GHz	21″ (2D mode)
	5″ @ 34 GHz	15″ (1D mode)
Time resolution	1s (steady)	∼ 2 min (2D, full disk)
	0.1 s (event)	∼ 10 s (2D, active region)
		14 ms (1D)
Sensitivity	400 K	1500 K
Imaging principle	Synthesis	Frequency scanning (112 MHz) + Earth rotation

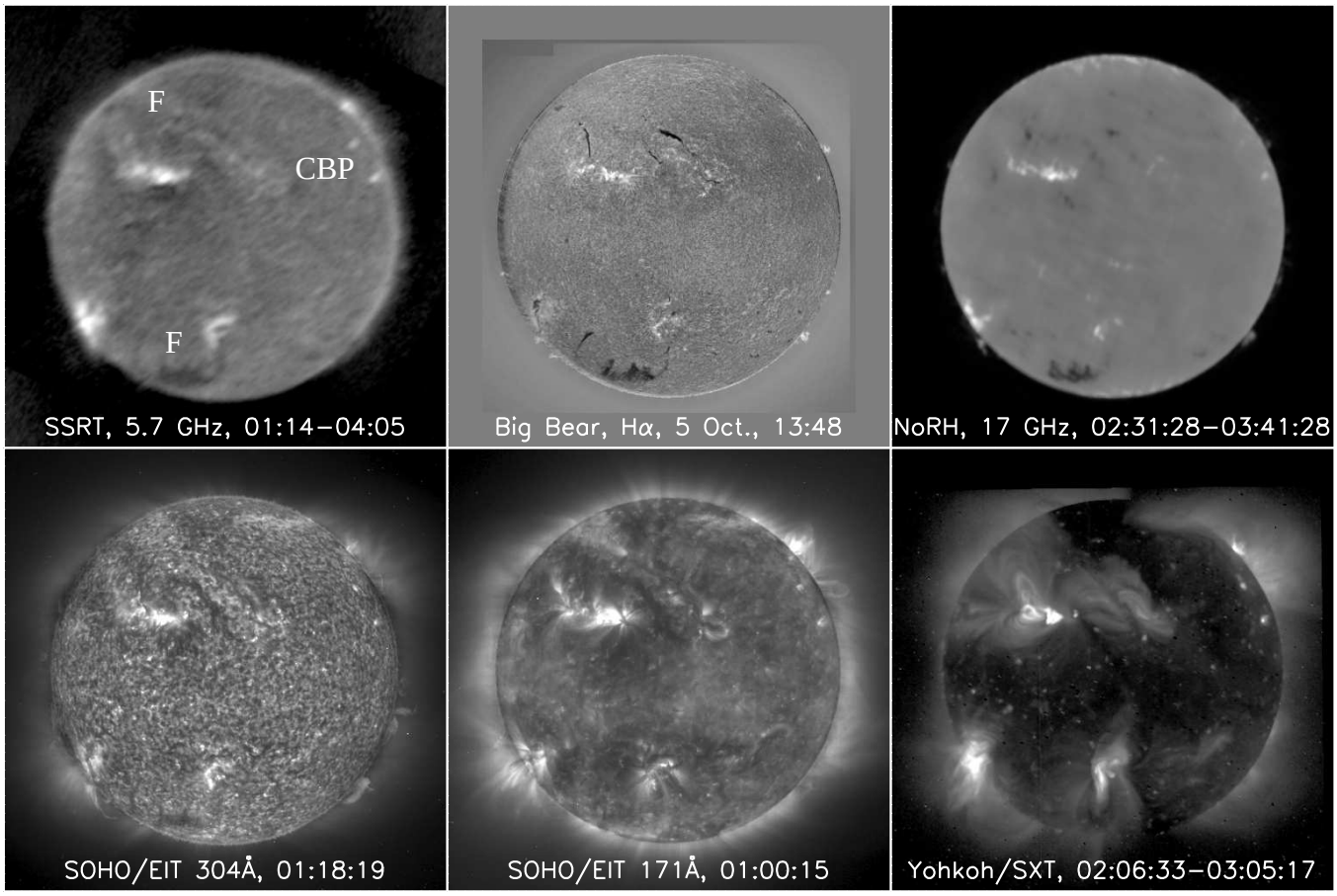

Fig. 3. Comparison of an SSRT Stokes *I* dirty map of 6 October 1997 with data from other spectral domains. All images are nonlinearly processed to make both bright sources and the quiet Sun pronounced. Solar North is up.

displayed to show both bright sources and the quiet Sun.

Optically thin bright features like emitting coronal loops above plages and coronal ("X-ray") bright points are visible in both SSRT and NoRH images. The SSRT map in Fig. 3 shows a wider range of brightness compared with the NoRH map at 17 GHz due to the greater contribution of coronal emissions at the lower frequency. The relation of brightness temperatures for such features is generally close to the frequency ratio squared, 8.8.

3.1. Filaments & Prominences

Filaments and prominences are pronounced in microwaves due to their low kinetic temperature and high density. Thus, they block brighter emission when observed on the solar disk, and produce well detectable own emission when observed against the sky.

Filaments and filament channels ("F" in Fig. 3) are supposed to be optically thick at both 5.7 and 17 GHz. Their brightness temperatures are usually close, which confirms

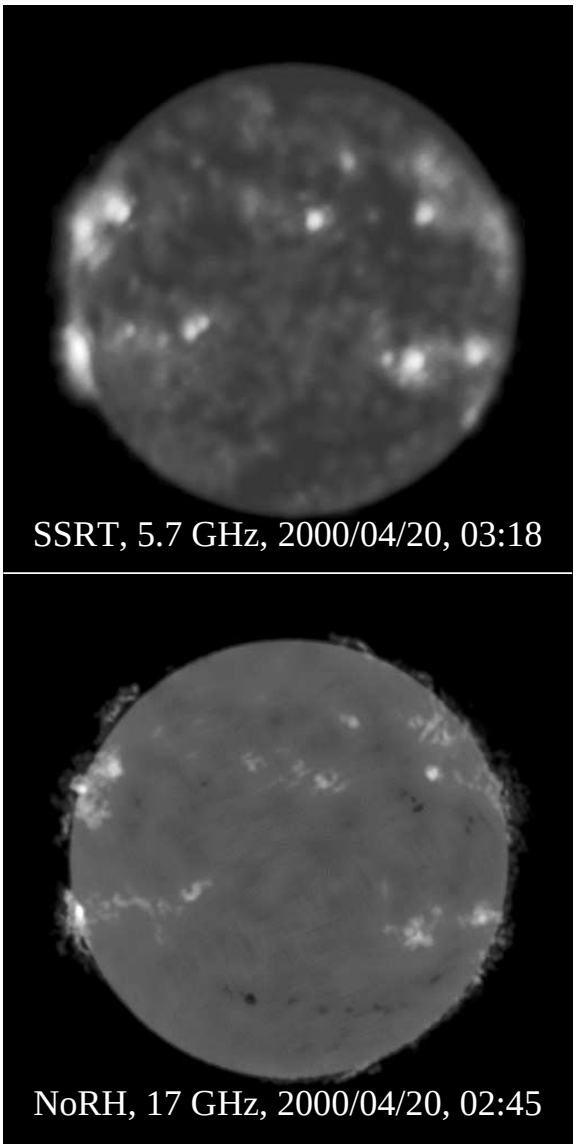

Fig. 2. SSRT clean image of April 20, 2000, and the corresponding NoRH image.

that. At 5.7 GHz, cool filaments and filament channels show higher contrast and more details. Some filaments not detectable with NoRH are nevertheless visible in SSRT maps (Zandanov and Lesovoi 1999). An apparent explanation of all these facts is the higher contrast with the quiet Sun ($T_{QS} = 16\,000$ K at 5.7 GHz and $T_{QS} = 10\,000$ K at 17 GHz). Filaments with higher kinetic temperature, about 10 000 K, are obviously not visible at 17 GHz, but still visible at 5.7 GHz.

Prominences are well observed with SSRT and NoRH, both quiescent and eruptive (Uralov et al. 2002, Grechnev et al. 2004a).

3.2. Coronal Bright Points

Coronal bright points (CBP), especially a pair localized close to the northwest limb in Fig. 3, are detectable in all images, and even in Hα filtergram. In SSRT images, they are usually well pronounced, and their brightness temperatures are typically some 10^4 K.

Analyses of simultaneous observations of CBPs at different frequencies does not show one-to-one correspondence between them. Besides coinciding CBPs, there are CBPs observed at one frequency, but absent at another one (Fig. 4). It is still not clear whether the differences are due to some physical properties of CBPs or the domains above which they are localized, or they are due to some observational aspects. Habbal et al. (1986) and Kundu et al. (1988) showed that properties of CBPs in the range of 1.5–5 GHz correspond to optically thin free-free emission. The same conclusion was made by Maksimov et al. (2001) for the observations with SSRT at 5.7 GHz and NoRH at 17 GHz. Thus, this emission mechanism is confirmed for CBPs in the frequency range of 1.5–17 GHz. Second, studying manifestations of CBPs at 5.7, 17 GHz, and in soft X-ray, Maksimov et al. (2001) concluded that some weak coronal bright points visible in other emissions are not pronounced in NoRH maps due to effects of the CLEAN routine. This also explains why the northern bright point of the pair is faint in NoRH image of Fig. 3 ($T_{B\,17} = 11\,900$ K).

3.3. Coronal Holes

Coronal holes are often visible in SSRT images. They are generally inhomogeneous, with brighter and darker portions (Krissinel et al. 2000). Due to this fragmentation, coronal holes are not as pronounced at 5.7 GHz as in soft X-ray images. Coronal holes are not distinct at 17 GHz, but sometimes they are manifest as fragmented bright features (Gopalswamy et al. 1998, Krissinel et al. 2000). To a first approximation, the more pronounced coronal contribution at 5.7 GHz (38% on the average, considering T_{QS}) is an apparent explanation of these facts. Detailed investigation of coronal holes at the two frequencies has revealed the following (Maksimov et al. 2004).

- Microwave observations confirm that coronal holes are inhomogeneous (cf., e.g., Chertok et al. 2002). The inhomogeneities have various sizes and shapes. Some of them are identified with features observed in other emissions, and some not.
- There are features within a hole and its vicinity whose brightness temperatures at both frequencies correlate: a) coronal bright points and diffuse brightenings, which are bright at both 5.7 and 17 GHz; b) filaments, which are dark at both 5.7 and 17 GHz.
- Maksimov et al. (2004) have found regions within coronal holes where, unlike features listed above, the brightness temperatures at 5.7 and 17 GHz anticorrelate. They are disposed radially. These regions are darkest at 5.7 GHz, but are not pronounced in either 195 Å, or Hα images. These regions dominate; hence, the image of a coronal hole resembles a negative of its image in extreme ultraviolet or in longer microwaves (Fig. 5).

For the enhanced brightness of coronal holes at 17 GHz

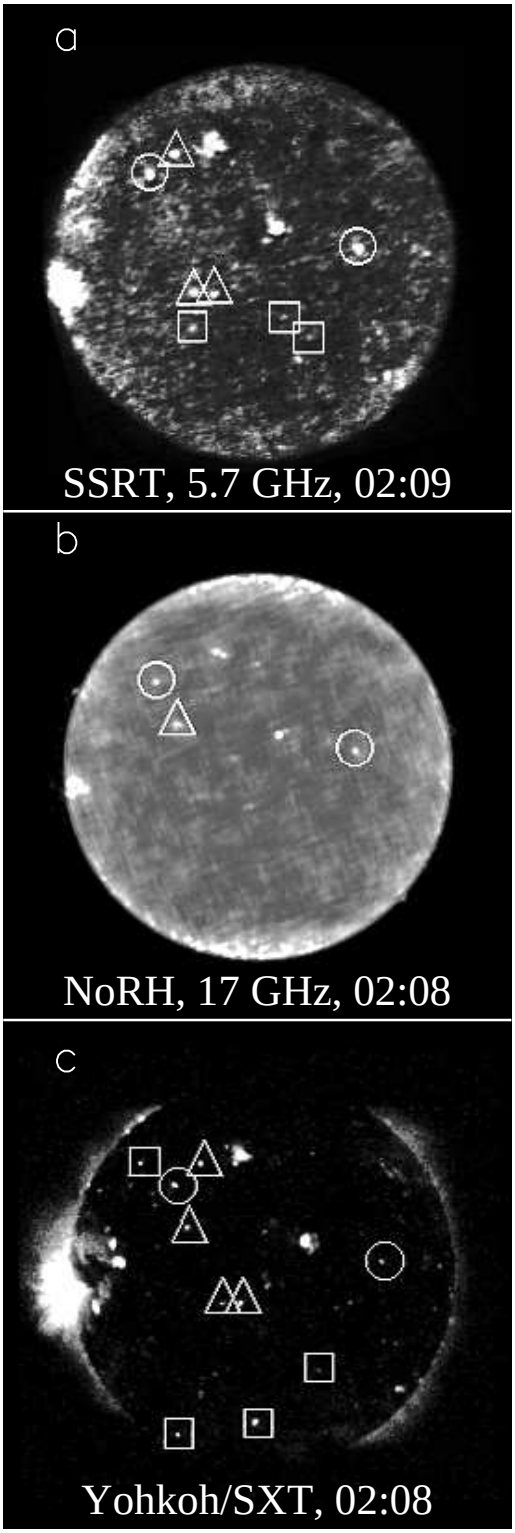

Fig. 4. Coronal bright points observed on June 3, 1996 with SSRT (a), NoRH (b), and *Yohkoh*/SXT (c). The selection criterion for CBPs is the excess of 3σ above the Sun's level. Circles mark CBPs observed in all images, triangles mark CBPs that have not all counterparts, squares mark CBPs with no counterparts.

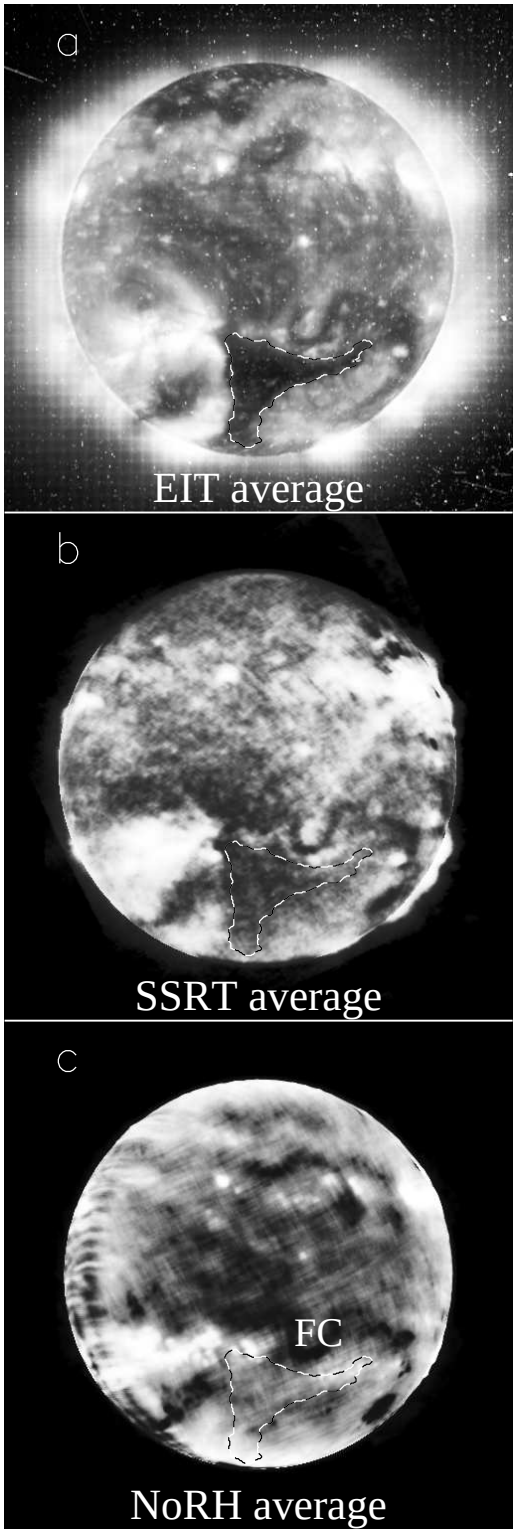

Fig. 5. A coronal hole observed during April 20–23, 1998: a) SOHO/EIT 195 Å, b) SSRT, c) NoRH images all averaged with their preliminary "derotation" to the same time of April 22, 06:00 UT. A dashed contour of the hole determined from the EIT image is superimposed on top of the SSRT and NoRH images. A filament channel is labeled "FC". Average brightness temperatures over the hole are $\langle T_{B\,5.7}\rangle = 15\,000$ K and $\langle T_{B\,17}\rangle = 11\,000$ K.

(at the chromospheric level), a mechanism can be responsible, which provides heating in the chromosphere (see, e.g., Gopalswamy et al. 1998), but simultaneously supplies cooling in the corona. The only known mechanism with such properties is dissipation of Alfvén waves. This mechanism requires further investigation, because there are some difficulties of their excitation and dissipation (see, e.g., Zirker 1993 and references therein).

The discussed radio observations at 5.7 and 17 GHz provide an identification criterion if a dark feature observed in radio images: if this feature is dark both at 5.7 and 17 GHz, it is a filament or a filament channel, not a coronal hole.

4. Studies of Magnetic Fields in the Corona

It was shown by Grechnev et al. (2003) that estimates of weak magnetic fields in the corona from SSRT polarization data for optically thin free-free emitting regions well correspond to a photospheric magnetogram (correlation of ≈ 0.95) even under very simple consideration (the magnetogram was convolved with the beam pattern of the SSRT). More rigorous approach permits to enhance significantly the correspondence of radio and magnetic measurements and to obtain new results, as shown further.

4.1. Coronal Arcades

Interesting and important bright features in SSRT and NoRH images are coronal arcades. Their studies promise diagnostics of thermal plasmas in coronal loops and disclosure of magnetic structures in the corona as well as estimates of the magnetic field strengths in them. Some of coronal arcades steadily persist for several days without conspicuous changes, and others, which form in the course of eruptions, gradually fade. The dominant emission mechanism of arcades is optically thin bremsstrahlung, but, especially in post-eruptive arcades, some non-thermal contribution can be present. It is important to identify the emission mechanism accurately, if we study the magnetic fields in the corona and try to estimate their strengths from polarization measurements. However, it can be impossible to do correctly from single-frequency observations. Two studies of coronal arcades carried out using NoRH and SSRT data along with observations in other spectral domains illustrate the above statements.

An arcade observed on November 23, 2000 in AR 9238 was analyzed by Grechnev et al. (2004b). The study has shown that the arcade formed in the course of an eruption, which occurred in an activity complex that included two active regions, AR 9231 and AR 9238. The eruptive event was triggered initially by a flux emergence in a remote site in AR 9231. Then the disturbance propagated along this active region, triggered activation and eruption of the filament, which was followed by a flare in AR 9238 and a CME. In that paper, the magnetic field in the arcade was studied, based on microwave data. The major emission mechanism in microwaves was assumed optically thin free-free emission.

However, some contribution of gyrosynchrotron emission from power-law electrons could significantly increase the degree of polarization. To evaluate its importance, Grechnev et al. (2004b) examined the flatness of the total intensity spectrum at lower frequencies using multi-frequency records from the RATAN-600 radio telescope.

The magnetic field strength in the arcade observed on November 23, 2000 was estimated from radio data to be $\sim$200 G at about 10 000 km, in accord with the extrapolation of the photospheric magnetic field into the corona.

Another arcade observed on October 22, 2001 (Fig. 6) formed also in the course of an eruption. Using multi-spectral data, Grechnev et al. (2004c) have estimated plasma parameters in the arcade several hours after the eruption at a height of ≈ 100 Mm: $N_e \sim 10^{10}$ cm^{-3} and $T_e \approx 6$ MK. Using deep averaging of NoRH data of 120 s for imaging, they have revealed a large-scale magnetic configuration surrounding the arcade high in the corona, in accord with the expected one from observations few days before as well as the potential-approximation extrapolation of the photospheric magnetic fields into the corona.

The arcade environment is negatively polarized both in NoRH and RATAN data at 17 GHz, thus delineating the magnetic configuration (x-mode, Fig. 7). A short-term appearance of the positive polarization in NoRH images southward of the arcade shows the presence there of a large-scale N-polarity magnetic field. The absence of the polarization in the brightest part of the arcade is due to the proximity of the opposite magnetic fields.

If the microwave emission mechanism would be optically thin bremsstrahlung exclusively, then the polarization measured of (10–12)% resulted in incomprehensible magnetic fields of $\sim$300 G at a height of $\sim$100 Mm. However, the total intensity spectrum of the microwave source measured with the RATAN-600 shows its non-thermal origin. Moreover, Fig. 6 shows that at 5.7 GHz, the arcade top is brighter with respect to the emitting source at its base than at 17 GHz, which could not be the case if the both sources were free-free emitting. Estimates show that an addition of 40%-polarized gyrosynchrotron emission with $T_B \sim$250 K can contribute the whole polarization observed. The extrapolation of the magnetic fields confirms the conclusions.

Grechnev et al. (2004c) also state a problem of long-term existence of the hot arcade high in the corona: either the magnetic field surrounding the arcade well exceeds 20 G at that height, or $\beta > 1$ both inside and outside the arcade. Note that a downflow observed in this case in soft X-rays, likely due to falling down remnants of the filament pre-ejected, can contribute to the balance of the arcade owing to the dynamic pressure of this downflow.

In summary, in those two papers, the importance was shown of the identification of the microwave emission mechanism from observations in a wide spectral range along with a technique to estimate contribution of non-thermal emissions to the polarization observed. Improper interpretation of the polarization measurements can result in well overestimated magnetic field strength in the corona due to non-thermal contributions.

It is worth to mention also coronal magnetography using

Fig. 6. A post-eruptive arcade observed on October 22, 2001 with the CORONAS-F/SPIRIT at 175 Å, NoRH, SSRT, and *Yohkoh*/SXT. The NoRH, SSRT, and *Yohkoh*/SXT images are averaged. The different ratio of the brightness in the top and at the base of the arcade at 5.7 and 17 GHz is due to non-thermal contribution at the arcade top.

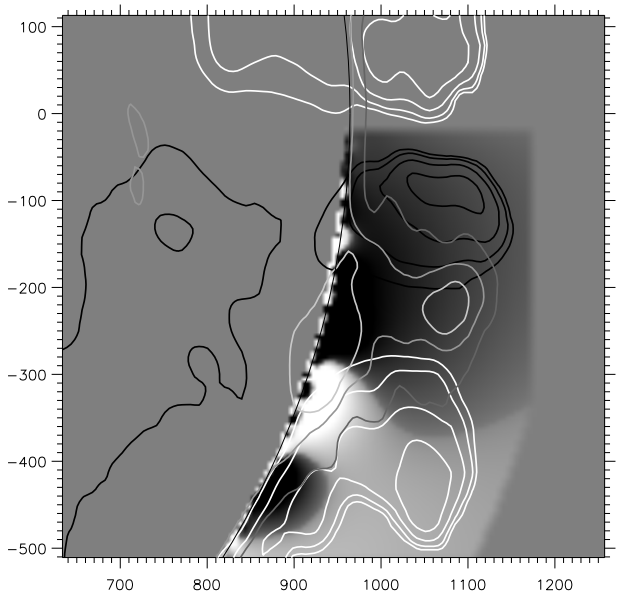

Fig. 7. A post-eruptive arcade observed on October 22, 2001: extrapolated in the potential approximation coronal magnetic fields (line-of-sight component) overlaid with gray contours of the NoRH total intensity and the degree of polarization (white contours positive). The axes show arc seconds from the solar disk center.

the polarization reversal effect in quasi-transverse magnetic field regions extensively addressed by Ryabov et al. (2003) and Ryabov (2004).

4.2. Identification of the type of a Radio Source

NoRH images of solar active regions (AR) show two types of quasi-stationary microwave sources. They are 1) compact sunspot-associated sources, and 2) neutral-line-associated sources (NLS), which are subdivided into weak, diffuse sources in simple bipolar regions, and rather bright, compact sources located in complex active regions in the vicinity of the inversion line of the radial component B_r of the coronal magnetic field. Uralov et al. (2000) first found compact NLS in NoRH images and classified them. SSRT observations of active regions containing NLS were studied earlier (e.g., Uralov et al. 1998), and those sources were regarded as predictors of powerful flares. Due to three times lower frequency, microwave sources in SSRT images are larger and usually cover sources visible in NoRH images.

It is rather difficult to recognize NLS in NoRH images. A direct comparison of microwave images of a solar active region with magnetograms of the longitudinal component of photospheric magnetic fields cannot correctly show *where* a microwave source is located within an active region. The main reason for that is the transformation of longitudinal magnetograms when we look at the solar surface non-radially. Due to the projection effect, magnetograms observed do not represent the true position of the magnetic field inversion line or the magnetic spot. Note also that NLS at 17 GHz are indistinguishable

from sunspot-associated gyroresonance sources in the degree of polarization, which can vary for sources of both types from small values up to 100%.

To avoid the projection effect and to detect NLS in NoRH maps, Uralov et al. (2004, 2005) propose a new procedure for the comparison of microwave images with the coronal magnetic field extrapolated from a single MDI magnetogram using the method by Rudenko (2001).

Figure 8 demonstrates results of this approach, representing 17 GHz intensity maps (background) along with extrapolated B_r magnetograms at a height of 2 000 km (contours) for AR 10486 on October 28–30, 2003. The magnetic inversion line is shown by thick solid line. The birth (solid arrows), displacement (dotted arrow), and persistence of compact neutral-line-associated sources along with development of the active region are seen. The birth and displacement of the NLS were accompanied by an X17.2 and X10 flares, correspondingly.

The investigation of the superactive period of October–November 2003 has shown that during that period, neutral-line-associated sources were not rare, but widespread at 17 GHz (Uralov et al. 2005).

5. Conclusion

Our overview emphasizes importance of observations with two radioheliographs. Putting additional constraints on physical conditions based on the observed quantities, microwave imaging data crucially enhance the reliability of results and consistency of interpretations. This is why microwave imaging data is a necessary constituent of observational data sets on solar phenomena.

Only observations at several radio frequencies assure identification of emission mechanisms and correct estimates of magnetic fields in the corona. In addition to traditional application of radio data, new research areas seem to appear: detection of flare-productive sites, coronal magnetography, non-local diagnostics of plasma parameters in height (in coronal holes), etc.

The results presented here have been possible due to the usage of microwave imaging data obtained with the solar dedicated radioheliographs NoRH and SSRT operating without interruption for over a decade.

Acknowledgments. We thank Pulkovo and Nobeyama Solar Groups and, especially, Prof. H. Nakajima and Prof. G. Gelfreikh for fruitful discussions and assistance. We are grateful to the Nobeyama Solar Group for the opportunity to participate this meeting and the hospitality. We thank the instrumental teams operating the Nobeyama Radioheliograph and the Siberian Solar Radio Telescope, SOHO/EIT & MDI, *Yohkoh*/SXT, and Big Bear Solar Observatory for data used here. This research was supported by the Russian Foundation for Basic Research (grants 03-02-16591 and 03-07-90087), the Russian Ministry of Education and Science (grant NSh-477.2003.2), the Russian Federal Program "Astronomy" and Lavrentiev's young scientist grant of SB RAS.

References

Chertok I.M., Obridko V.N., Mogilevsky E.I. et al. 2002, ApJ 567, 1225

Felli M., Lang K.R., Willson R.F. 1981, ApJ 247, 325

Gelfreikh G.B., Pilyeva N.A., Ryabov B.I. 1997, Sol. Phys. 170, 253

Gopalswamy N., Shibasaki K., DeForest C.E. et al. 1998, in Synoptic Solar Physics, ed. K.S. Balasubramanian, J.W. Harvey, D.M. Rabin, ASP Conf. Ser. 140, p363

Grechnev V.V., Lesovoi S.V., Smolkov G.Ya., Krissinel B.B., Zandanov V.G., Altyntsev A.T., Kardapolova N.N., Sergeev R.Y., Uralov A.M., Maksimov V.P., Lubyshev B.I. 2003, Sol. Phys. 216, 239

Grechnev V.V., Uralov A.M., Zandanov V.G., Baranov N.Y., Lesovoi S.V. 2004, Observations of Eruptive Events with Two Radioheliographs, SSRT and NoRH. Nobeyama Symp. 2004 "Solar Physics with the Nobeyama Radioheliograph", http://solar.nro.nao.ac.jp/meeting/nbym04/index.html; 2005, PASJ, in preparation

Grechnev V.V., Zandanov V.G., Uralov A.M., Maksimov V.P., Rudenko G.V., Borovik V.N., Gelfreikh G.B., Grigorieva I.Y., Medar V.G., Korzhavin A.N. 2004, Sol. Phys., in press

Grechnev V.V., Borovik V.N., Bugaenko O.I., Bogachev S.A., Grigorieva I.Y., Kuzin S.V., Lesovoi S.V., Livshits M.A., Pertsov A.A., Rudenko G.V., Slemzin V.A., Stepanov A.I., Shibasaki K., Uralov A.M., Zandanov V.G., Zhitnik I.A. Observations of a posteruptive arcade on October 22, 2001 with CORONAS-F, other spaceborne telescopes, and in microwaves. Nobeyama Symp. 2004 "Solar Physics with the Nobeyama Radioheliograph", http://solar.nro.nao.ac.jp/meeting/nbym04/index.html; 2005, PASJ, in preparation

Habbal S.R., Ronan R.S., Withbroe G.L., Shevgaonkar R.K., Kundu M.R. 1986, ApJ 306, 740

Krissinel B.B., Kuznetsova S.M., Maksimov V.P., Prosovetsky D.V., Grechnev V.V., Stepanov A.P., Shishko L.F. 2000, PASJ 52, 909

Kundu M.R. 1985, Sol. Phys. 100, 491

Kundu M.R., Schmahl E.J., Fu Q.-J. 1988, ApJ 325, 905

Maksimov V.P., Prosovetskii D.V., Krissinel B.B. 2001, Astron. Letters 27, 181

Maksimov V.P., Prosovetsky D.V., Grechnev V.V., Krissinel B.B., Shibasaki K. 2004, On the relation of brightness temperatures in coronal holes at 5.7 and 17 GHz. Nobeyama Symp. 2004 "Solar Physics with the Nobeyama Radioheliograph", http://solar.nro.nao.ac.jp/meeting/nbym04/index.html; 2005, PASJ, in preparation

Nakajima H., Nishio M., Enome S., Shibasaki K., Takano T., Hanaoka Y., Torii C., Sekiguchi H., Bushimata T., Kawashima S., Shinohara N., Irimajiri Y., Koshiishi H., Kosugi T., Shiomi Y., Sawa M., Kai K. 1994, Proc. IEEE 82(5), 705

Rudenko G.V. 2001, Sol. Phys. 198, 5

Ryabov B.I., Nindos A., Shibasaki K., Maksimov V.P., Lesovoi S.V., Pevtsov A.A. 2003, Fall Meeting AGU 2003, abst. #SH42B-0508

Ryabov B.I. Coronal magnetograms of solar active regions derived from polarization inversion in microwaves. 2004, Nobeyama Symp. 2004 "Solar Physics with the Nobeyama Radioheliograph", http://solar.nro.nao.ac.jp/meeting/nbym04/index.html;

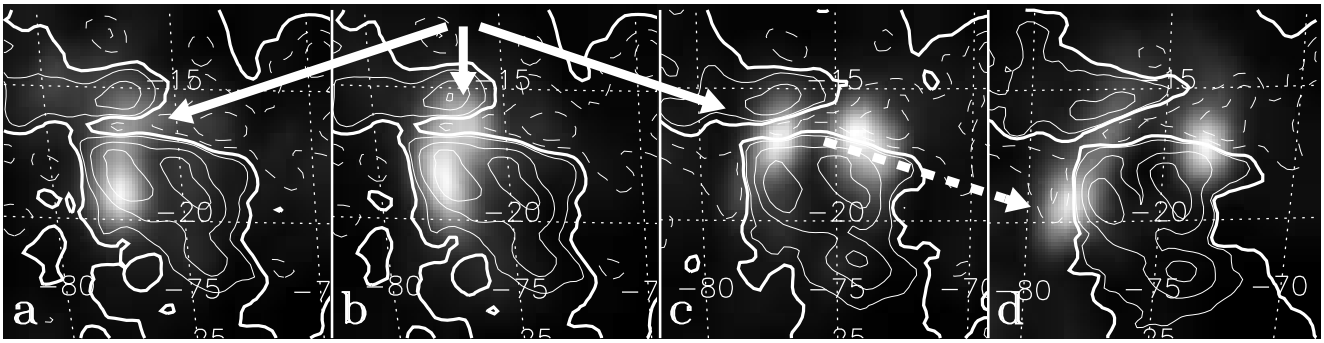

Fig. 8. 17 GHz intensity maps (background) and extrapolated B_r magnetograms (contours) of October 28, 03:10 (a) and 05:00 UT (b), October 29 (c), and 30 (d). Solid contours show positive polarity, dotted—negative. Magnetic inversion line is shown by thick solid line. One can see the birth (solid arrows) and persistence of compact neutral-line-associated sources. The arrows point out the birth site (solid) and the displacement (dashed) of the NLS.

this issue.
Smolkov G.Ia., Pistolkors A.A., Treskov T.A., Krissinel B.B., Putilov V.A. 1986, Ap&SS 119, 1
Uralov A.M., Sych R.A., Shchepkina V.L., Zubkova G.N., Smolkov G.Ya. 1998, Sol. Phys. 183, 359
Uralov A.M., Nakajima H., Zandanov V.G., Grechnev V.V. 2000, Sol. Phys. 197, 275
Uralov A.M., Lesovoi S.V., Zandanov V.G., Grechnev V.V. 2002, Sol. Phys. 208, 69
Uralov A.M., Rudenko G.V. 2004, Comparison of 5.7 and 17 GHz solar images with extrapolated magnetograms of coronal magnetic field. Active regions of the October/November 2003 period and forecast of powerful solar flares. Nobeyama Symp. 2004 "Solar Physics with the Nobeyama Radioheliograph", http://solar.nro.nao.ac.jp/meeting/nbym04/index.html; PASJ, 2005, in preparation
Uralov A.M., Rudenko G.V., Rudenko I.G. 2005, J. Geophys. Res., submitted
Zandanov V.G., Lesovoi S.V. 1999, Proc. Nobeyama Symp., Kiyosato, Japan, Oct. 27–30, 1998, ed. T. S. Bastian, N. Gopalswamy, K. Shibasaki, NRO Report 479, p37
Zirker J.B. 1993, Sol. Phys. 148, 43